
Emergent Semantic Role Understanding in Language Models

Carla Griffiths
University College London

Mirco Musolesi
University College London
University of Bologna

Abstract

Understanding how linguistic structure emerges in language models is central to interpreting what these systems learn from data and how much supervision they truly require. In particular, semantic role understanding (“who did what to whom”) is a core component of meaning representation, yet it remains unclear whether it arises from pre-training alone or depends on task-specific fine-tuning.

We study whether semantic role understanding emerges during language model pre-training or requires task-specific fine-tuning. We freeze decoder-only transformers and train linear probes to extract semantic roles, using performance to infer whether role information is already encoded in pre-training or learned during adaptation. Across model scales, we find that frozen representations contain substantial semantic role information, with performance improving but not fully matching fine-tuned models. This indicates partial but incomplete emergence from pre-training alone. We show that semantic role structure emerges from language modeling objectives, but its internal implementation shifts toward more distributed representations as model scale increases.

1 Introduction

Understanding the emergence of linguistic structure in Large Language Models (LLMs) is essential for characterizing what they learn from data and the extent to which supervision is required. In particular, *semantic role understanding* (“who did what to whom”) Gildea and Jurafsky [2002] is a core component of meaning representation, yet it remains unclear whether it arises from pre-training alone or depends on task-specific fine-tuning. Indeed, LLMs trained on next-token prediction have demonstrated capabilities that arguably extend beyond simple text completion [Brown et al., 2020, Radford et al., 2019]. Building on the transformer architecture [Vaswani et al., 2017] and pre-training paradigms pioneered by BERT [Devlin et al., 2019] and ELMo [Peters et al., 2018a], modern LLMs learn rich contextual representations that generalize across tasks [Howard and Ruder, 2018, Ruder et al., 2019]. This success has prompted extensive investigation into what linguistic knowledge these models acquire [Rogers et al., 2020, Jawahar et al., 2019, Liu et al., 2019].

Our central hypothesis is that *semantic role understanding emerges from pre-training alone*, even at small model scales, and that this emergence can be detected and characterized through probing and targeted ablations. Semantic role labeling (SRL) is the task of identifying the predicate-argument structure of sentences, determining “who did what to whom, when, where, and how” [Palmer et al., 2010]. For example, given the sentence “The dog took a long walk in the park.” QA-SRL generates questions like “Who took a walk?” (Agent: the dog), “What did someone take?” (Patient: a long walk), and “Where did someone take a walk?” (Location: the park). This formulation is particularly suitable for probing language models, as it requires no explicit linguistic annotation schema and naturally maps to extractive question answering.

How can we tell if a model learned semantic roles during pre-training rather than during task-specific training? We freeze the pre-trained model and train only a simple linear layer to extract answers. If this frozen model performs well, semantic role information was encoded during pre-training; if the frozen model performs poorly, the capability must be learned during fine-tuning. In particular, our experimental design addresses three core questions:

1. *Does emergence of semantic role understanding occur?* Do frozen model representations contain sufficient information for semantic role identification?
2. *Is emergence of semantic role understanding scale-dependent?* At what model scale (if any) does the gap between frozen-probe and full-fine-tuning performance narrow significantly?
3. *How is semantic role information organized?* Can we identify how semantic roles are encoded inside the model and the intrinsic neural mechanisms? Do these representations form a clear, interpretable structure?

Beyond linear probing, we perform mechanistic analysis to understand how semantic roles are represented. Using PCA and t-SNE [van der Maaten and Hinton, 2008] visualization of layer activations, following similar approaches in LLM interpretability [Gurnee and Tegmark, 2024], we find that semantic roles form distinct clusters in representation space (Figure 6), with separation increasing in deeper layers. We identify individual neurons in the feed-forward layers that selectively activate for specific semantic roles (e.g., “*Agent* neurons”, “*Location* neurons”) and causally validate their importance through targeted ablation experiments. These role-selective neurons exhibit functional co-activation patterns, with within-role correlations exceeding those across roles. This separation generally increases with layer depth.

We train decoder-only transformer models from scratch on WikiText-103 [Merity et al., 2016], spanning four scales from 0.4M to 57M transformer parameters. We evaluate using QA-SRL [He et al., 2015], a task that reformulates semantic role labeling as question answering (e.g., asking “Who took a walk?” to identify the *Agent* role). Our results characterize the emergence threshold for semantic role understanding and contribute to the broader understanding of what linguistic capabilities arise from language modeling objectives alone.

This work makes the following contributions:

- We present a systematic methodology for testing emergence of semantic role understanding using linear probing on frozen LLM representations. We provide empirical evidence characterizing the relationship between model scale and the frozen-probe vs. full-fine-tuning performance gap on QA-SRL.
- We introduce a temporal analysis framework using Centered Kernel Alignment (CKA) to track how representations evolve during fine-tuning relative to the pre-trained (null) model.
- We identify role-selective neurons through PCA/t-SNE visualization and neuron ablation, discovering that semantic roles cluster in representation space and that role-selective neurons show increasing co-activation separation with layer depth.
- We conduct role-conditioned neuron ablations revealing scale-dependent neural reorganization: *Agent*-selective neurons transition from causally important in small models to interfering in large models, while *Time*-selective neurons remain consistently causal across scales.

Code and trained models with checkpoint weights are available from the authors upon request.

2 Related Work

Emergence in Language Models. *Emergent abilities* in language models refer to capabilities that appear suddenly as models scale [Wei et al., 2022]. Scaling laws predict smooth improvements in perplexity [Kaplan et al., 2020, Hoffmann et al., 2022], but task performance can exhibit sharp transitions. However, recent work questions whether emergence is a genuine phase transition or a measurement artifact: Schaeffer et al. [2023] argue that nonlinear metrics like exact match create the appearance of sudden capability acquisition, while Snell et al. [2024] show that fine-tuning can unlock capabilities present but inaccessible in smaller models. These findings suggest that “emergence” may

reflect our evaluation methods rather than underlying model organization. Our work addresses this limitation by using continuous F1 metrics and linear probing, which provide a more fine-grained view of capability development. Rather than asking *when* semantic role understanding appears, we characterize *how much* is present at each scale, distinguishing between information encoded during pre-training versus information created during fine-tuning.

Probing Classifiers. Probing classifiers analyze what information is encoded in neural representations [Belinkov, 2022]. The BERTology literature [Rogers et al., 2020, Jawahar et al., 2019, Clark et al., 2019, Liu et al., 2019, Vulić et al., 2020, Peters et al., 2018b] has extensively applied probing, finding that lower layers encode syntax while higher layers capture semantics. Linear probes are preferred to constrain capacity [Hewitt and Liang, 2019]. Our methodology extends probing by comparing frozen performance to full fine-tuning, measuring how much information is already present versus must be learned.

Semantic Role Labeling. SRL has evolved from feature-based classifiers [Gildea and Jurafsky, 2002, Pradhan et al., 2005] to neural approaches [Zhou and Xu, 2015, He et al., 2017, Marcheggiani and Titov, 2017, Roth and Lapata, 2016, Strubell et al., 2018], with pre-trained models providing strong features [Shi and Lin, 2019]. We use QA-SRL [He et al., 2015, FitzGerald et al., 2018], which reformulates SRL as question answering without requiring explicit PropBank schemas, making it suitable for probing emergence from language exposure alone.

Linguistic Structure in LLMs. Structural probes find syntactic tree structure in LLM representations [Hewitt and Manning, 2019], while layer-wise analysis shows that lower layers encode surface features and higher layers capture abstract semantics [Tenney et al., 2019, Peters et al., 2018b, Liu et al., 2019]. Building on static [Mikolov et al., 2013, Pennington et al., 2014] and contextualized embeddings [Peters et al., 2018a, Devlin et al., 2019], our work examines semantic *role* structure specifically, using ablations to establish causal relationships between neurons and semantic functions.

Mechanistic Interpretability. Recent work reverse-engineers neural network algorithms: feed-forward layers as key-value memories [Geva et al., 2021], circuit-level task analysis [Wang et al., 2023, Conmy et al., 2023, Olsson et al., 2022], and sparse autoencoders for monosemantic features [Elhage et al., 2022, Bricken et al., 2023, Cunningham et al., 2024, Templeton et al., 2024]. Our work differs by training models from scratch for controlled scale manipulation, focusing on QA-SRL as a well-defined semantic task, and combining probing with neuron ablation to test causal necessity.

3 Methods

3.1 Model Architecture

We train decoder-only transformer language models following the GPT-2 & GPT-3 architecture [Radford et al., 2019]. All models use learned positional embeddings, pre-layer normalization, GELU activations, and a feed-forward expansion factor of 4. We use the `bert-base-uncased` tokenizer ($\sim 30\text{K}$ vocabulary), held fixed across all four scales following standard practice in scaling-law studies [Kaplan et al., 2020, Hoffmann et al., 2022]. Scaling vocabulary with model size would confound transformer capacity with tokenization granularity; under our design, the same input distribution is presented to all four transformers, so the only varying quantity is the transformer’s depth and width. We tie token embedding weights to the LM head during pre-training. We train four model configurations spanning approximately three orders of magnitude in parameter count (Table 1).

3.2 Pre-training

All models are pre-trained on WikiText-103 [Merity et al., 2016] using the standard causal language modeling objective. WikiText-103 contains approximately 103 million tokens of Wikipedia articles, providing exposure to diverse factual content and linguistic structures without explicit QA formatting.

The pre-training objective is next-token prediction with cross-entropy loss:

$$\mathcal{L}_{\text{pretrain}} = - \sum_{t=1}^T \log P(x_t | x_{<t}; \theta) \tag{1}$$

Table 1: Model configurations and parameter counts. Total parameters include embeddings (token + positional); transformer parameters exclude embeddings to enable comparison across vocabulary sizes.

Config	Layers	Hidden	Heads	Transformer	Total
Tiny	2	128	2	0.4M	4.4M
Small	4	256	4	3.2M	11.1M
Base	6	512	8	18.9M	34.8M
Medium	8	768	12	56.7M	80.5M

where x_t is the token at position t and θ represents model parameters.

3.3 QA-SRL Fine-tuning Task

After pre-training, models are fine-tuned (or probed) on QA-SRL [He et al., 2015]. Each example consists of a sentence, a predicate within that sentence, a question about that predicate’s semantic role, and an answer span. During preprocessing, we skip examples where the answer text appears multiple times in the context (ambiguous spans), filtering approximately 9% of examples. The model receives the concatenated input:

[question] [SEP] [sentence]

and must predict start and end positions for the answer span within the sentence. Critically, we maintain causal attention during fine-tuning (matching pre-training), ensuring that any performance gap between frozen and fine-tuned models reflects differences in learned representations rather than attention pattern mismatch. With the question preceding the sentence, the model can attend to the full question when processing each sentence token.

We add a QA head consisting of two linear projections from the hidden dimension to scalar logits for start and end positions:

$$\mathbf{s} = \mathbf{H}\mathbf{w}_{\text{start}} \tag{2}$$

$$\mathbf{e} = \mathbf{H}\mathbf{w}_{\text{end}} \tag{3}$$

where $\mathbf{H} \in \mathbb{R}^{L \times d}$ is the sequence of hidden states and $\mathbf{w}_{\text{start}}, \mathbf{w}_{\text{end}} \in \mathbb{R}^d$ are learned projection vectors.

3.4 Linear Probing Protocol

Overview Our protocol distinguishes two related claims that prior probing work has often conflated. Information is *decodable* when a linear probe extracts it from a frozen pre-trained model, establishing the information is present somewhere in the model’s parameters and inputs together. It is *emergent* from pre-training when the information lives in the pre-trained transformer weights, separately from trainable embeddings or fine-tuned layers, evidenced by a gap over an architecture-matched random baseline and corroborated by per-layer probes on pure pre-trained representations with zero embedding adaptation (Section 4.4). Decodability is the weaker, established property; emergence under controlled conditions is the stronger claim our design tests. Note that the token embedding is a position-independent lookup table (identical outputs for “the dog bit the child” and “the child bit the dog”), so role resolution under the frozen probe must come from the frozen transformer’s cross-position attention rather than from embedding adaptation alone. We use two fine-tuning regimes described below.

Full Fine-tuning and Frozen Linear Probe. In *full fine-tuning*, all model parameters (transformer layers and QA head) are updated during QA-SRL training. This establishes an upper bound on task performance for each model scale. In the case of the *frozen linear probe*, all transformer block parameters and positional embeddings are frozen; only the token embeddings and QA head ($\mathbf{w}_{\text{start}}, \mathbf{w}_{\text{end}}$) are trained. This tests whether the answer span information is encoded in the frozen transformer representations. We deliberately keep the token embedding matrix trainable rather than frozen: the input format [question] [SEP] [sentence] relies on [SEP] as a structural separator,

and [SEP] is a BERT-tokenizer artifact that was never seen in a separator role during causal language-model pre-training, so a fully frozen embedding matrix would prevent the model from parsing the input format and confound representation quality with input-format adaptation rather than test it. Embedding updates can still propagate through the frozen layers, creating a residual “adaptation effect” that we analyze separately via per-layer probes with zero embedding adaptation (Section 4.4) and a stricter frozen-embedding (SEP-only) ablation in Appendix J, where only [SEP] and the QA head update. The gap between full fine-tuning and frozen probe performance quantifies how much semantic role information must be learned during fine-tuning versus how much is already present from pre-training.

Random Baseline. To establish a performance floor, we also evaluate a *random baseline*: a randomly initialized (untrained) model whose token embeddings and QA head are trained on QA-SRL while the transformer blocks remain at random initialization. This is a capacity-matched comparator for the frozen probe (same trainable parameters, only the source of the transformer weights differs), which isolates the contribution of the pre-trained transformer from any contribution of trainable embeddings.

Normalized Emergence Score. We define a normalized emergence score that accounts for the random baseline floor:

$$\text{Emergence}_{\text{norm}} = \frac{F1_{\text{frozen}} - F1_{\text{random}}}{F1_{\text{full}} - F1_{\text{random}}}. \quad (4)$$

A score near 1.0 indicates strong emergence (frozen probe captures most of what full fine-tuning achieves above chance), while a score near 0.0 indicates the frozen probe performs no better than random initialization. We also report the raw gap $\Delta_{\text{emergence}} = F1_{\text{full}} - F1_{\text{frozen}}$ (while less rigorous, the raw score is more intuitive).

3.5 Temporal CKA Analysis

To understand how representations evolve during fine-tuning, we employ Centered Kernel Alignment (CKA) [Kornblith et al., 2019] to measure representational similarity across training checkpoints. For activation matrices $\mathbf{X}, \mathbf{Y} \in \mathbb{R}^{n \times d}$, linear CKA is:

$$\text{CKA}(\mathbf{X}, \mathbf{Y}) = \frac{\|\mathbf{Y}^\top \mathbf{X}\|_F^2}{\|\mathbf{X}^\top \mathbf{X}\|_F \|\mathbf{Y}^\top \mathbf{Y}\|_F}. \quad (5)$$

We save checkpoints at each epoch and compute CKA between each fine-tuning checkpoint and the pre-trained (*null*) model. A decrease in CKA_{null} indicates representational drift from pre-training during fine-tuning.

4 Results

4.1 Overview

We present results across four model scales: Tiny (0.4M), Small (3.2M), Base (18.9M), and Medium (56.7M transformer parameters). We report the F1 Score on the QA-SRL validation step, defined as the token-level overlap between predicted and gold answer spans, computed as the harmonic mean of precision and recall. In the evaluation, we apply context masking to constrain predictions to the sentence region only, preventing the model from predicting spans within the question or special tokens. Table 2 summarizes performance across three experimental conditions for each model size: random baseline (untrained LLM with trained QA head), frozen linear probe (pre-trained LLM frozen, only QA head trained), and full fine-tuning (all parameters updated).

4.2 Analysis of the Emergence of Semantic Role Understanding

All models show positive emergence, with frozen probes consistently outperforming random baselines (Figure 1b). To understand what drives the emergence score, we decompose it into two components:

- $\Delta_{\text{pre}} = F1_{\text{frozen}} - F1_{\text{random}}$: pre-training’s contribution above chance;
- $\Delta_{\text{ft}} = F1_{\text{full}} - F1_{\text{frozen}}$: fine-tuning’s additional contribution.

Table 2: Results on QA-SRL semantic role labeling across model scales. All models show positive emergence, with frozen pre-trained representations encoding semantic role information accessible to linear probes. F1 (%) shown as mean \pm std over 5 random seeds; emergence score $E = \Delta_{\text{pre}} / (\Delta_{\text{pre}} + \Delta_{\text{ft}})$.

	Tiny (0.4M)	Small (3.2M)	Base (18.9M)	Medium (56.7M)
Random baseline	24.2 \pm 0.6	25.3 \pm 0.1	25.5 \pm 0.2	26.1 \pm 0.5
Frozen (linear probe)	36.4 \pm 0.8	39.6 \pm 0.7	43.6 \pm 0.5	44.7 \pm 0.5
Full fine-tuning	44.6 \pm 0.4	53.3 \pm 0.7	63.8 \pm 0.4	65.8 \pm 0.7
Emergence E	0.60 \pm 0.06	0.51 \pm 0.03	0.47 \pm 0.02	0.47 \pm 0.02

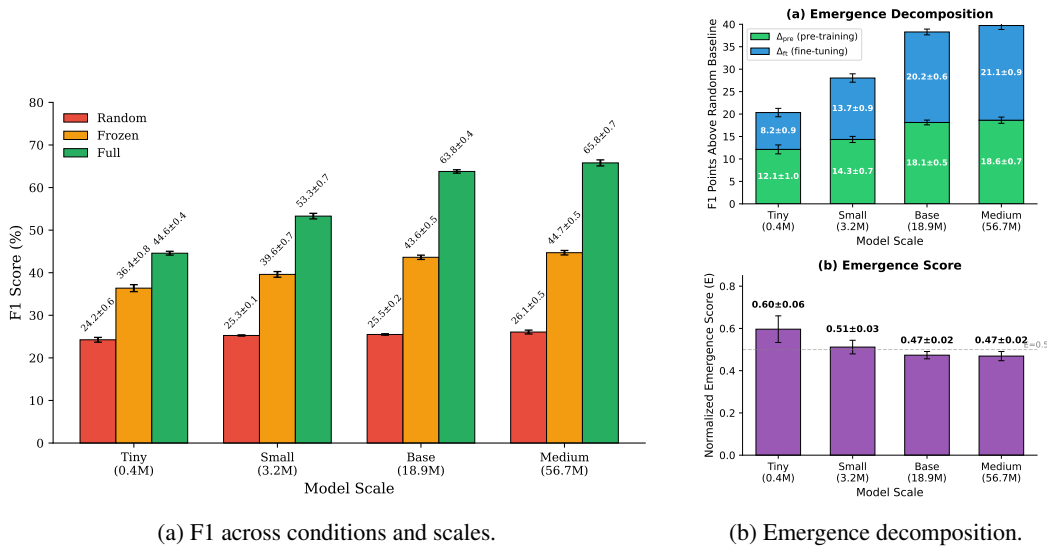


Figure 1: Frozen probes extract semantic role information without any model adaptation. (a) We compare three conditions: *Random baseline* (untrained model + QA head only), *Frozen probe* (pre-trained model frozen, only QA head trained), and *Full fine-tuning* (all parameters updated). The frozen probe substantially outperforms random at all scales. (b) Decomposing performance into $\Delta_{\text{pre}} = F1_{\text{frozen}} - F1_{\text{random}}$ (pre-training above chance) and $\Delta_{\text{ft}} = F1_{\text{full}} - F1_{\text{frozen}}$ (fine-tuning’s additional contribution): pre-training contributes 12–19 F1 points across scales while fine-tuning’s contribution grows with scale (8–21 points). The normalized emergence score $E = \Delta_{\text{pre}} / (\Delta_{\text{pre}} + \Delta_{\text{ft}})$ decreases with scale because fine-tuning becomes increasingly effective relative to a relatively constant pre-training contribution. Values: mean \pm std over 5 random seeds.

The normalized emergence score is defined as $E = \Delta_{\text{pre}} / (\Delta_{\text{pre}} + \Delta_{\text{ft}})$. Examining these components reveals that pre-training’s contribution (Δ_{pre}) ranges from 12.1 to 18.6 F1 points (12.1 \pm 1.0, 14.3 \pm 0.7, 18.1 \pm 0.5, 18.6 \pm 0.7 for Tiny through Medium), showing consistent gains across all scales. In contrast, fine-tuning’s contribution (Δ_{ft}) grows substantially with scale (8.2 \pm 0.9, 13.7 \pm 0.9, 20.2 \pm 0.6, 21.1 \pm 0.9 points). The normalized emergence score decreases with scale because fine-tuning becomes increasingly effective at larger scales while pre-training’s contribution stays roughly constant. The score thus reflects the fraction of task performance that comes “for free” from pre-training, and this fraction shrinks as fine-tuning scales up.

These results show that semantic role information is decodable from frozen pre-trained representations across all scales, with a consistent 12–19 F1 gap above the architecture-matched random baseline. The frozen-probe condition, however, leaves the token embedding matrix trainable, conflating emergence in transformer weights with task-driven embedding adaptation; we disentangle the two next.

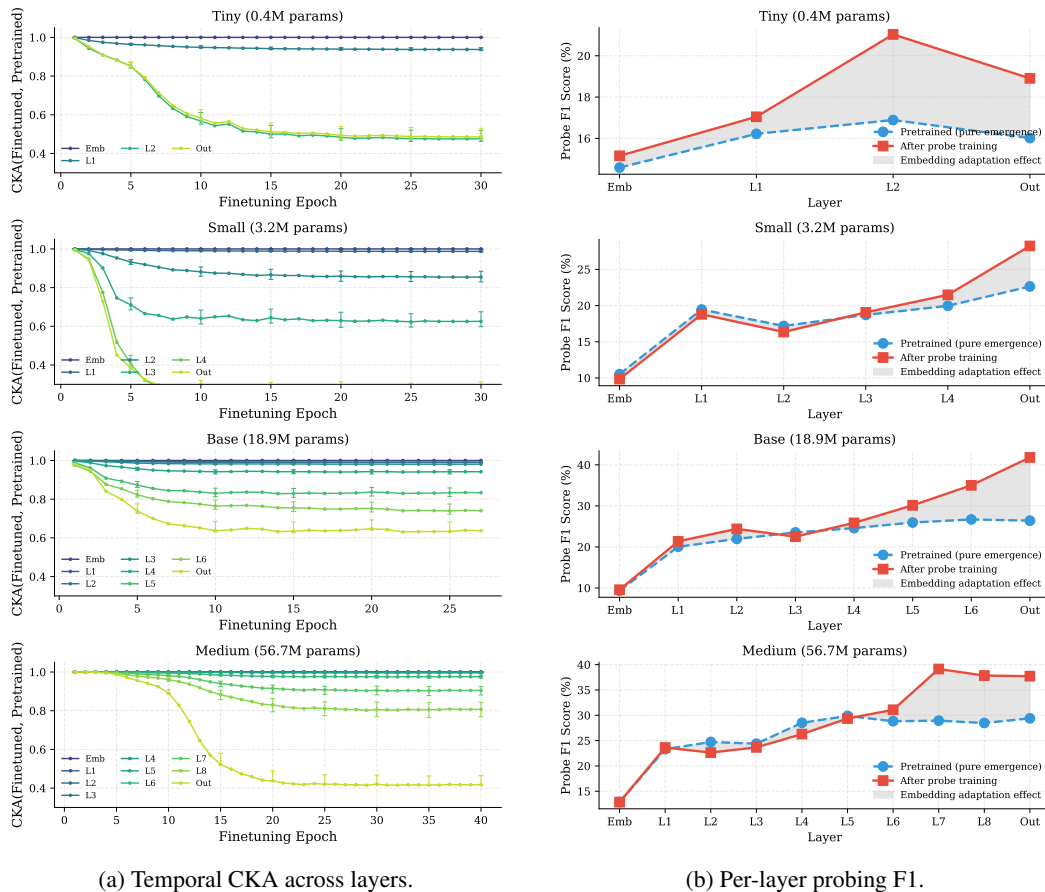


Figure 2: Representational changes during fine-tuning, and isolation of pre-training from adaptation. (a) Centered Kernel Alignment (CKA) between each fine-tuning epoch and the original pre-trained model: deeper layers (darker lines) diverge most, dropping to $CKA \approx 0.25$ to 0.49 , while early layers remain stable. (b) Per-layer linear probes comparing *Pure pre-trained* (blue dashed; before any SRL training) and *After probe training* (red solid). Gray region marks adaptation effect. Probes are trained on 500 samples and measure layer-specific linear separability, so absolute values differ from Table 2. F1 on pure pre-trained representations ranges from 10 to 26% across scales, isolating information present in fixed transformer weights.

4.3 Representational Changes During Fine-tuning

To understand how representations evolve during fine-tuning, we perform Centered Kernel Alignment (CKA) analysis comparing each fine-tuning epoch against the pre-trained model. CKA analysis shows that full fine-tuning substantially reorganizes representations, with deeper layers diverging most from pre-training (CKA dropping to 0.25 to 0.49; Figure 2a). This raises a key question: is semantic role information *created* during fine-tuning, or already present in pre-trained representations?

4.4 Isolating Emergence from Adaptation

To determine whether semantic role information is encoded during pre-training (emergence) versus created during fine-tuning (adaptation), we train linear probes on pre-trained representations before any task-specific training. We compare this to probes trained after frozen probe training. Semantic role information is present in pure pre-trained representations: linear probes achieve 10 to 26% F1 across layers and scales before any SRL training (Figure 2b). This confirms that emergence occurs even at small scales; predicate-argument structure is encoded during pre-training rather than created during task-specific adaptation. As a stricter control, a frozen-embedding (SEP-only) ablation

Table 3: Role-conditioned neuron ablation. We ablate each role’s selective neurons and measure *that role’s* F1 specifically (i.e., F1 computed only on validation examples whose gold answer carries that role label, not overall task F1 from Table 2). Negative Δ confirms causal importance for that semantic role; positive Δ in larger models indicates interference. F1 baselines for each role differ from overall F1 because role-specific subsets are smaller relative to the whole population.

Role Ablated	Tiny		Small		Base		Medium	
	F1	Δ	F1	Δ	F1	Δ	F1	Δ
<i>Agent</i> \rightarrow <i>Agent</i> F1	0.0%	-2.9%	11.5%	-1.9%	14.4%	+1.9%	24.0%	+14.4% [†]
<i>Time</i> \rightarrow <i>Time</i> F1	2.4%	-2.4%	9.8%	-4.9%	22.0%	-2.4%	7.3%	-4.9%
<i>Location</i> \rightarrow <i>Location</i> F1	0.0%	0.0%	0.0%	0.0%	3.6%	0.0%	3.6%	0.0%
<i>Manner</i> \rightarrow <i>Manner</i> F1	3.8%	+3.8%	0.0%	0.0%	3.8%	0.0%	3.8%	+3.8%

[†]Positive Δ suggests interference or redundant representations in larger models.

isolates the residual transformer contribution and is statistically significant at our two largest scales ($p = 0.004$, $p = 0.002$; full results in Appendix J).

4.5 Neuron-Level Dynamics

Overview. We identify role-selective neurons using PCA. First, we run PCA on feed-forward activations across all validation samples, then test whether principal components separate semantic roles using ANOVA F-statistics. For each discriminative principal component ($p < 0.0001$), we extract the top 5 neurons with the highest absolute loadings, selecting up to 20 role-selective neurons per layer across all discriminative principal components. We refer to neurons selective for specific PropBank roles: *Agent* neurons (selective for ARG0, the actor/doer of an action), *Time* neurons (selective for ARGM-TMP, temporal modifiers like “yesterday” or “during the meeting”), *Location* neurons (ARGM-LOC), and *Manner* neurons (ARGM-MNR) (PropBank definitions in Section E).

PCA and t-SNE Visualizations. PCA and t-SNE visualizations of final-layer feed-forward activations (Appendix D, Figure 6) reveal that activations show partial organization by PropBank semantic role, with ARG0-Agent showing the clearest separation; the first two principal components explain only 14.8% of variance, indicating that semantic roles are encoded in a higher-dimensional subspace not fully captured by linear projections. Named-role-selective neurons (*Agent*, *Location*, *Manner*) concentrate in early layers (L0–L1; see Table 9 and Figure 4 in Appendix C), suggesting role encoding begins early in the network. To causally validate neuron importance, we set the weights of PCA-identified neurons to 0 in the *pretrained* model, then finetune on QA-SRL and evaluate. This tests whether specific neurons are necessary (not just correlated) for learning semantic roles. We perform role-conditioned neuron ablation: ablating role X ’s neurons and measuring role X ’s specific F1 (Table 3, for full results see Table 4).

Role-conditioned Analysis. The role-conditioned results reveal scale-dependent neural organization. *Time* neurons show consistent causal importance across all scales, with ablations reducing *Time* F1 by -2.4% to -4.9% . Smaller models (Tiny: -2.9% , Small: -1.9%) show clear dependence on *Agent*-selective neurons, while larger models show improved performance when these neurons are ablated (Base: $+1.9\%$, Medium: $+14.4\%$). This reversal suggests that larger models develop redundant or interfering representations, and that ablating putatively *Agent*-selective neurons removes this interference. *Location* and *Manner* neurons show minimal or no causal effects across scales ($\Delta \approx 0$), suggesting these roles lack specialized neurons or are represented distributionally. The consistent *Time* neuron effects, combined with scale-dependent *Agent* effects, demonstrate that role-selective neurons exist but reorganize with capacity. The *Agent*-neuron sign attenuation replicates on GPT-2 (124M, 355M; Appendix F) and Pythia (70M, 160M, 410M; Appendix G) with random-neuron controls confirming role-specificity, and component-level circuit analysis across all six models shows the same concentrated-to-distributed transition (Appendix H), Figure 3).

Cross-role Interference and Co-activation. Two distinct patterns of interference emerge at scale, both absent in small models. (i) *Time*-neuron ablation in larger models reduces *Time* F1 (-4.9%) but

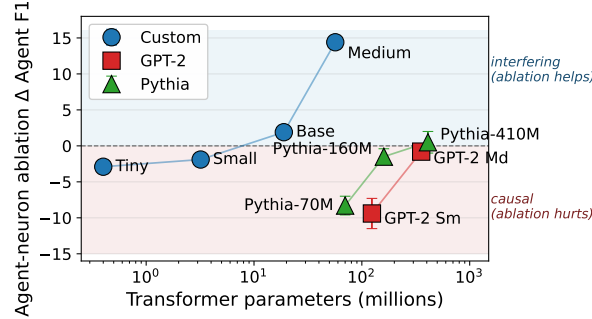


Figure 3: Ablation Δ Agent F1 (role-specific, matching Table 3; not overall F1) across 9 parameter configurations. The custom-model trajectory (blue) crosses zero between Small and Base; GPT-2 and Pythia show the same pattern. Error bars: \pm std over 5 seeds.

improves overall F1 (+1.0%): the role-specific neurons are causally helpful for their own role yet suppress more frequent roles, so removing them improves overall F1 via weighted averaging. (ii) Medium-scale Agent-neuron ablation improves both Agent F1 (+14.4%) and overall F1 (+5.8%): putatively Agent-selective neurons have become net interfering even for their own role, consistent with redundant or miscoordinated representations at scale. Pairwise correlations between PCA-identified neurons show same-role neurons more correlated than different-role neurons ($\rho_{\text{within}} \approx 0.24$ vs. $\rho_{\text{across}} \approx 0.10$), consistent with distributed, overlapping representations. Per-role critical layers, overall ablation F1, and the power-law fit are in Appendix C and Appendix A.

Limitations. *Single-seed ablations:* role-conditioned and overall neuron-ablation results on custom models (Tables 3, 4, 8) are point estimates from one fine-tuning run per (model, role) pair; the qualitative Agent-neuron sign-attenuation pattern holds across 5-seed replications on GPT-2 and Pythia. *Dataset quality:* the original QA-SRL dataset [He et al., 2015] achieves $\sim 72.4\%$ recall against expert annotations [FitzGerald et al., 2018], which may underestimate absolute F1; our analyses focus on the emergence gap, where systematic annotation noise cancels. *Data-constrained scaling:* WikiText-103’s $\sim 103\text{M}$ tokens give a tokens-to-parameters ratio of ~ 1.8 for Medium versus the Chinchilla-optimal ~ 20 [Hoffmann et al., 2022]; despite this, Medium achieves the highest fine-tuned F1 ($65.8\% \pm 0.7\%$), and reported emergence is conservative as Medium remains under-converged (Appendix I). The Agent-neuron sign reversal replicates on fully-trained GPT-2 and Pythia (Appendices F–G). *Model scale:* custom models reach 57M transformer parameters; GPT-2 (355M) and Pythia (410M) remain small relative to massive commercialized LLMs.

5 Conclusion

Summary. We have studied whether semantic role understanding emerges during language model pre-training and presented an investigation of how semantic role understanding emerges in language models across four scales (0.4M to 57M transformer parameters). We have showed that pre-training contributes 12–19 F1 above architecture-matched random initialization across scales, with layer-wise probing on pure pre-trained representations confirming encoding of predicate-argument structure. Moreover, feed-forward neurons activate selectively for semantic roles, with co-activation separation generally increasing with layer depth. Role-conditioned ablations reveal consistent importance of time-related neurons across all scales while neurons associated to the agent show scale-dependent effects: causal in smaller models but improving performance when ablated in larger models, suggesting neural reorganization as model size increases. Critically, cross-role interference emerges in larger models. This scale-dependent reorganization shows that larger models develop complex neuron interactions absent in smaller models.

Implications. Our work has important implications for understanding language models. First, role-selective neurons demonstrate that emergent linguistic capabilities can partially localize, suggesting that interpretability methods can identify meaningful structure in emergent behaviors. Second, cross-role interference in larger models demonstrates that language models do not necessarily implement clean one-to-one mappings between individual neurons and specific functions. Third,

the scale-dependent neural reorganization, where *Agent* neurons transition from causally important to interfering, challenges the assumption that circuits identified in smaller models will retain their function at larger scales. Fourth, our frozen probing methodology suggests that semantic role understanding emerges from pre-training on natural language across model scales.

Acknowledgments and Disclosure of Funding

This work investigates the emergence of semantic role understanding through assessing what capabilities are learned during pre-training versus fine-tuning. We see no ethical issues with this work, as understanding how semantic understanding emerges helps demystify LLM capabilities. Our experiments required approximately 860 GPU hours for the custom models plus approximately 200 GPU hours for the GPT-2 and Pythia replications; we will release the full model weights with checkpoints to reduce redundant computation. We thank Modal for a GPU grant that enabled the majority of these experiments to be run at no cost.

References

- Daniel Gildea and Daniel Jurafsky. Automatic labeling of semantic roles. In *Computational Linguistics*, volume 28, pages 245–288, 2002.
- Tom Brown, Benjamin Mann, Nick Ryder, Melanie Subbiah, Jared D Kaplan, Prafulla Dhariwal, Arvind Neelakantan, Pranav Shyam, Girish Sastry, Amanda Askell, et al. Language models are few-shot learners. In *Proceedings of the 34th Conference on Neural Information Processing Systems (NeurIPS’20)*, 2020.
- Alec Radford, Jeffrey Wu, Rewon Child, David Luan, Dario Amodei, and Ilya Sutskever. Language models are unsupervised multitask learners. *OpenAI Blog*, 1(8):9, 2019.
- Ashish Vaswani, Noam Shazeer, Niki Parmar, Jakob Uszkoreit, Llion Jones, Aidan N Gomez, Łukasz Kaiser, and Illia Polosukhin. Attention is all you need. In *Proceedings of the 30th Conference on Neural Information Processing Systems (NeurIPS’17)*, 2017.
- Jacob Devlin, Ming-Wei Chang, Kenton Lee, and Kristina Toutanova. BERT: Pre-training of deep bidirectional transformers for language understanding. In *Proceedings of the 2019 Conference of the North American Chapter of the Association for Computational Linguistics (NAACL’19)*, 2019.
- Matthew E. Peters, Mark Neumann, Mohit Iyyer, Matt Gardner, Christopher Clark, Kenton Lee, and Luke Zettlemoyer. Deep contextualized word representations. In *Proceedings of the 2018 Conference of the North American Chapter of the Association for Computational Linguistics (NAACL’18)*, 2018a.
- Jeremy Howard and Sebastian Ruder. Universal language model fine-tuning for text classification. In *Proceedings of the 56th Annual Meeting of the Association for Computational Linguistics (ACL’18)*, 2018.
- Sebastian Ruder, Matthew E. Peters, Swabha Swayamdipta, and Thomas Wolf. Transfer learning in natural language processing. *Proceedings of the 2019 Conference of the North American Chapter of the Association for Computational Linguistics (NAACL’19): Tutorial Abstracts*, 2019.
- Anna Rogers, Olga Kovaleva, and Anna Rumshisky. A primer in BERTology: What we know about how BERT works. *Transactions of the Association for Computational Linguistics*, 8:842–866, 2020.
- Ganesh Jawahar, Benoît Sagot, and Djamé Seddah. What does BERT learn about the structure of language? In *Proceedings of the 57th Annual Meeting of the Association for Computational Linguistics (ACL’19)*, 2019.
- Nelson F. Liu, Matt Gardner, Yonatan Belinkov, Matthew E. Peters, and Noah A. Smith. Linguistic knowledge and transferability of contextual representations. In *Proceedings of the 2019 Conference of the North American Chapter of the Association for Computational Linguistics (NAACL’19)*, 2019.

- Martha Palmer, Daniel Gildea, and Nianwen Xue. Semantic role labeling. *Synthesis Lectures on Human Language Technologies*, 3(1):1–103, 2010.
- Laurens van der Maaten and Geoffrey Hinton. Visualizing data using t-SNE. *Journal of Machine Learning Research*, 9:2579–2605, 2008.
- Wes Gurnee and Max Tegmark. Language models represent space and time. In *Proceedings of the 12th International Conference on Learning Representations (ICLR’24)*, 2024.
- Stephen Merity, Caiming Xiong, James Bradbury, and Richard Socher. Pointer sentinel mixture models. *arXiv preprint arXiv:1609.07843*, 2016.
- Luheng He, Mike Lewis, and Luke Zettlemoyer. Question-answer driven semantic role labeling: Using natural language to annotate natural language. In *Proceedings of the 2015 Conference on Empirical Methods in Natural Language Processing (EMNLP’15)*, 2015.
- Jason Wei, Yi Tay, Rishi Bommasani, Colin Raffel, Barret Zoph, Sebastian Borgeaud, Dani Yogatama, Maarten Bosma, Denny Zhou, Donald Metzler, et al. Emergent abilities of large language models. *Transactions on Machine Learning Research*, 2022.
- Jared Kaplan, Sam McCandlish, Tom Henighan, Tom B Brown, Benjamin Chess, Rewon Child, Scott Gray, Alec Radford, Jeffrey Wu, and Dario Amodei. Scaling laws for neural language models. *arXiv preprint arXiv:2001.08361*, 2020.
- Jordan Hoffmann, Sebastian Borgeaud, Arthur Mensch, et al. Training compute-optimal large language models. *arXiv preprint arXiv:2203.15556*, 2022.
- Rylan Schaeffer, Brando Miranda, and Sanmi Koyejo. Are emergent abilities of large language models a mirage? In *Proceedings of the 37th Conference on Neural Information Processing Systems (NeurIPS’23)*, 2023.
- Charlie Snell, Eric Wallace, Dan Klein, and Sergey Levine. Predicting emergent capabilities by fine-tuning. In *Proceedings of the 2024 Conference on Language Modeling (COLM’24)*, 2024.
- Yonatan Belinkov. Probing classifiers: Promises, shortcomings, and advances. *Computational Linguistics*, 48(1):207–219, 2022.
- Kevin Clark, Urvashi Khandelwal, Omer Levy, and Christopher D Manning. What does BERT look at? an analysis of BERT’s attention. In *Proceedings of the 2019 ACL Workshop BlackboxNLP: Analyzing and Interpreting Neural Networks for NLP*, 2019.
- Ivan Vulić, Edoardo Maria Ponti, Robert Litschko, Goran Glavaš, and Anna Korhonen. Probing pretrained language models for lexical semantics. In *Proceedings of the 2020 Conference on Empirical Methods in Natural Language Processing (EMNLP’20)*, 2020.
- Matthew E. Peters, Mark Neumann, Luke Zettlemoyer, and Wen-tau Yih. Dissecting contextual word embeddings: Architecture and representation. In *Proceedings of the 2018 Conference on Empirical Methods in Natural Language Processing (EMNLP’18)*, 2018b.
- John Hewitt and Percy Liang. Designing and interpreting probes with control tasks. In *Proceedings of the 2019 Conference on Empirical Methods in Natural Language Processing (EMNLP’19)*, 2019.
- Sameer Pradhan, Wayne Ward, Kadri Hacioglu, James H. Martin, and Daniel Jurafsky. Semantic role labeling using different syntactic views. In *Proceedings of the 43rd Annual Meeting of the Association for Computational Linguistics (ACL’05)*, 2005.
- Jie Zhou and Wei Xu. End-to-end learning of semantic role labeling using recurrent neural networks. In *Proceedings of the 53rd Annual Meeting of the Association for Computational Linguistics (ACL’15)*, 2015.
- Luheng He, Kenton Lee, Mike Lewis, and Luke Zettlemoyer. Deep semantic role labeling: What works and what’s next. In *Proceedings of the 55th Annual Meeting of the Association for Computational Linguistics (ACL’17)*, 2017.

- Diego Marcheggiani and Ivan Titov. Encoding sentences with graph convolutional networks for semantic role labeling. In *Proceedings of the 2017 Conference on Empirical Methods in Natural Language Processing (EMNLP'17)*, 2017.
- Michael Roth and Mirella Lapata. Neural semantic role labeling with dependency path embeddings. In *Proceedings of the 54th Annual Meeting of the Association for Computational Linguistics (ACL'16)*, 2016.
- Emma Strubell, Patrick Verga, Daniel Andor, David Weiss, and Andrew McCallum. Linguistically-informed self-attention for semantic role labeling. In *Proceedings of the 2018 Conference on Empirical Methods in Natural Language Processing (EMNLP'18)*, 2018.
- Peng Shi and Jimmy Lin. Simple BERT models for relation extraction and semantic role labeling. *arXiv preprint arXiv:1904.05255*, 2019.
- Nicholas FitzGerald, Julian Michael, Luheng He, and Luke Zettlemoyer. Large-scale QA-SRL parsing. In *Proceedings of the 56th Annual Meeting of the Association for Computational Linguistics (ACL'18)*, 2018.
- John Hewitt and Christopher D Manning. A structural probe for finding syntax in word representations. In *Proceedings of the 2019 Conference of the North American Chapter of the Association for Computational Linguistics (NAACL'19)*, 2019.
- Ian Tenney, Dipanjan Das, and Ellie Pavlick. BERT rediscovers the classical NLP pipeline. In *Proceedings of the 57th Annual Meeting of the Association for Computational Linguistics (ACL'19)*, 2019.
- Tomas Mikolov, Ilya Sutskever, Kai Chen, Greg S Corrado, and Jeff Dean. Distributed representations of words and phrases and their compositionality. In *Advances in Neural Information Processing Systems 26 (NeurIPS'13)*, 2013.
- Jeffrey Pennington, Richard Socher, and Christopher D Manning. GloVe: Global vectors for word representation. In *Proceedings of the 2014 Conference on Empirical Methods in Natural Language Processing (EMNLP'14)*, 2014.
- Mor Geva, Roei Schuster, Jonathan Berant, and Omer Levy. Transformer feed-forward layers are key-value memories. In *Proceedings of the 2021 Conference on Empirical Methods in Natural Language Processing (EMNLP'21)*, 2021.
- Kevin Wang, Alexandre Variengien, Arthur Conmy, Buck Shlegeris, and Jacob Steinhardt. Interpretability in the wild: A circuit for indirect object identification in GPT-2 small. In *Proceedings of the 11th International Conference on Learning Representations (ICLR'23)*, 2023.
- Arthur Conmy, Augustine Mavor-Parker, Aengus Lynch, Stefan Heimersheim, and Adrià Garriga-Alonso. Towards automated circuit discovery for mechanistic interpretability. In *Proceedings of the 37th Conference on Neural Information Processing Systems (NeurIPS'23)*, 2023.
- Catherine Olsson, Nelson Elhage, Neel Nanda, et al. In-context learning and induction heads. In *Transformer Circuits Thread*, 2022. Anthropic.
- Nelson Elhage, Tristan Hume, Catherine Olsson, et al. Toy models of superposition. *Transformer Circuits Thread*, 2022. Anthropic.
- Trenton Bricken, Adly Templeton, Joshua Batson, et al. Towards monosemanticity: Decomposing language models with dictionary learning. *Transformer Circuits Thread*, 2023. Anthropic.
- Hoagy Cunningham, Aidan Ewart, Logan Riggs, Robert Huben, and Lee Sharkey. Sparse autoencoders find highly interpretable features in language models. In *Proceedings of the 12th International Conference on Learning Representations (ICLR'24)*, 2024.
- Adly Templeton, Tom Conerly, Jonathan Marcus, et al. Scaling monosemanticity: Extracting interpretable features from Claude 3 Sonnet. *Transformer Circuits Thread*, 2024. Anthropic.

- Simon Kornblith, Mohammad Norouzi, Honglak Lee, and Geoffrey Hinton. Similarity of neural network representations revisited. In *Proceedings of the 36th International Conference on Machine Learning (ICML'19)*, 2019.
- Ilya Loshchilov and Frank Hutter. Decoupled weight decay regularization. In *Proceedings of the 7th International Conference on Learning Representations (ICLR'19)*, 2019.
- Stella Biderman, Hailey Schoelkopf, Quentin Anthony, et al. Pythia: A suite for analyzing large language models across training and scaling. In *Proceedings of the 40th International Conference on Machine Learning (ICML'23)*, 2023.
- Leo Gao, Stella Biderman, Sid Black, Laurence Golding, Travis Hoppe, Charles Foster, Jason Phang, Horace He, Anish Thite, Noa Nabeshima, et al. The Pile: An 800GB dataset of diverse text for language modeling. *arXiv preprint arXiv:2101.00027*, 2020.

A Full Neuron Ablation Results

Table 4 shows overall F1 impact when ablating PCA-identified role-selective neurons. These results aggregate across all semantic roles in the validation set and reflect weighted averaging due to unbalanced role distributions (*Theme*: 55.8%, *Agent*: 20.8%, *Time*: 8.2%, *Location*: 5.6%, others: 9.6%). For more interpretable causal validation, see Table 3, which measures role-specific F1 impact.

Table 4: Overall neuron ablation results across all semantic roles. We ablate PCA-identified role-selective neurons before fine-tuning and measure overall F1 impact. Baseline F1 scores in column headers (e.g., “Tiny (2.2%)”) show pre-ablation overall F1 *on the role-conditioned evaluation subset used in Table 3*, not overall F1 on the full validation set from Table 2. These overall F1 changes reflect weighted averaging across unbalanced role distributions and may not align with role-specific effects (see Section 4.5 and Table 3). Values are single-seed point estimates.

Ablation	Tiny (2.2%)		Small (6.2%)		Base (7.6%)		Medium (5.4%)	
	F1	Δ	F1	Δ	F1	Δ	F1	Δ
<i>Agent</i>	1.2%	-1.0%	5.0%	-1.2%	7.4%	-0.2%	11.2%	+5.8% [†]
<i>Location</i>	2.2%	0.0%	5.0%	-1.2%	8.0%	+0.4%	6.6%	+1.2%
<i>Time</i>	1.2%	-1.0%	6.0%	-0.2%	7.4%	-0.2%	6.4%	+1.0%
<i>Manner</i>	2.4%	+0.2%	5.8%	-0.4%	8.8%	+1.2%	10.0%	+4.6% [†]

[†]Positive Δ in larger models reflects cross-role interference (Section 4.5).

B Training Hyperparameters

All experiments were conducted on NVIDIA GPUs using Modal’s cloud infrastructure. Models were implemented in PyTorch 2.0 with mixed-precision training (FP16) where applicable. We generated the analysis for Figures 3-8 locally using Metal Performance Shaders on an M4 MacBook Pro.

B.1 Compute Resources

Table 5: Compute configuration and estimated training times per model. Base and Medium models were migrated to faster GPUs mid-training due to time constraints (Base: epoch 78, Medium: epoch 68).

Config	GPU	VRAM	Pretrain Time	Finetune Time	Total GPU Hours
Tiny	A10G	24GB	~48h	~1h	~49h
Small	A10G	24GB	~72h	~1h	~73h
Base	A10G → H200	24/80GB	~336h	~4h	~340h
Medium	A100 → H200	80GB	~390h	~10h	~400h

B.2 Pre-training Hyperparameters

B.3 Fine-tuning Hyperparameters

All fine-tuning results are reported as mean±std over 5 random seeds (42, 1042, 2042, 3042, 4042).

B.4 Optimizer Configuration

All models use the AdamW optimizer [Loshchilov and Hutter, 2019] with the following settings:

- $\beta_1 = 0.9$, $\beta_2 = 0.999$.
- Weight decay: 0.01.
- Learning rate schedule: Constant learning rate with early stopping.

Table 6: Pre-training hyperparameters for each model configuration.

Hyperparameter	Tiny	Small	Base	Medium
Sequence Length	512	512	512	512
Batch Size	64	48	32	96
Gradient Accumulation	1	1	1	1
Learning Rate	5×10^{-4}	2×10^{-4}	2×10^{-4}	1×10^{-4}
Warmup Steps	500	500	1000	2000
Max Epochs	200	200	200	200
Early Stopping Patience	20	20	20	20
Dropout Rate	0.05	0.1	0.1	0.1
Samples per Epoch	200K	400K	800K	1.5M

Table 7: QA-SRL fine-tuning hyperparameters for each model configuration.

Hyperparameter	Tiny	Small	Base	Medium
Sequence Length	512	512	512	512
Batch Size	64	48	32	32
Learning Rate (Full Finetune)	4×10^{-5}	2×10^{-5}	1×10^{-5}	1×10^{-5}
Learning Rate (Frozen Probe)	1×10^{-3}	1×10^{-3}	1×10^{-3}	1×10^{-3}
Max Epochs	30	30	30	30
Early Stopping Patience	8	8	8	8

- Gradient clipping: Max norm 1.0.
- Label smoothing: $\alpha = 0.1$ (pre-training cross-entropy loss).

B.5 Temporal CKA Analysis Configuration

For the temporal CKA analysis described in Section 3.5:

- Probe set size: 500 examples from QA-SRL validation set.
- Checkpoint frequency: Every fine-tuning epoch.
- Activation pooling: Mean pooling over sequence length (excluding padding).
- CKA variant: Linear CKA with centered activations.

C Neuron-Level Analysis Details

Table 8: Critical layer for each role: layer whose ablation gives the largest *role-specific* $\Delta F1$ (computed on the subset of validation examples carrying that role label, not overall F1). Values in parentheses are role-specific $\Delta F1$ for that layer. Single-seed point estimates.

	Tiny	Small	Base	Med
LOC	L0 (−17%)	L1 (−12%)	L1 (−6%)	L0 (−13%)
MNR	L1 (−18%)	L3 (−24%)	L0 (−11%)	L5 (−5%)
ARG2	L0 (−14%)	L0 (−4%)	L0 (−12%)	L0 (−5%)
TMP	L1 (−6%)	L1 (−9%)	L4 (−3%)	L0 (−6%)

We identify neurons with selectivity scores $> 10\times$ the mean activation for specific roles:

Table 9 lists the most selective neurons for each semantic role. This specialization emerges naturally from language model pre-training without explicit role supervision.

Table 9: Top role-selective neurons in the Small model. Selectivity is computed as the ratio of mean activation for the target role to mean activation across all roles.

Role	Layer	Neuron Index	Selectivity
<i>Agent</i>	0	41	40.7×
<i>Agent</i>	1	343	28.3×
<i>Location</i>	0	180	31.5×
<i>Location</i>	1	530	36.2×
<i>Time</i>	0	665	22.1×
<i>Time</i>	1	817	19.8×
<i>Time</i>	1	826	18.4×
<i>Manner</i>	0	412	15.2×
<i>Manner</i>	2	891	14.7×

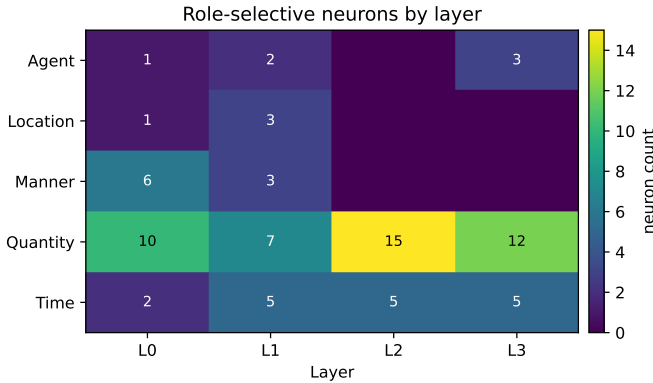


Figure 4: Layer \times role distribution of the top-20 PCA-identified selective neurons per layer in the Small (3.2M) model. Cell values are neuron counts. Named PropBank-style roles (*Agent*, *Location*, *Manner*) concentrate in early layers (L0–L1); *Time* neurons appear in every layer; *Quantity* neurons dominate the top-20 cap throughout the network.

C.1 Co-activation Correlation Methodology

The co-activation correlations (ρ) reported in Section 4.5 are computed as follows:

- Collect activations:** For each QA-SRL validation sample, we extract the feed-forward layer activations $\mathbf{a} \in \mathbb{R}^{d_{\text{ff}}}$ at each layer.
- Filter to role-selective neurons:** We retain only neurons identified as role-selective via PCA (see Section 4.5), yielding activation vectors $\mathbf{a}_{\text{selective}} \in \mathbb{R}^{n_{\text{selective}}}$.
- Compute pairwise Pearson correlations:** For each pair of role-selective neurons (i, j), we compute the Pearson correlation coefficient across all N validation samples:

$$\rho_{ij} = \frac{\sum_{k=1}^N (a_i^{(k)} - \bar{a}_i)(a_j^{(k)} - \bar{a}_j)}{\sqrt{\sum_{k=1}^N (a_i^{(k)} - \bar{a}_i)^2} \sqrt{\sum_{k=1}^N (a_j^{(k)} - \bar{a}_j)^2}} \quad (6)$$

where $a_i^{(k)}$ is the activation of neuron i on sample k .

- Partition by role relationship:** We separate correlations into two groups based on whether the neuron pair shares the same semantic role:

$$\rho_{\text{within}} = \{\rho_{ij} : \text{role}(i) = \text{role}(j)\} \quad (7)$$

$$\rho_{\text{across}} = \{\rho_{ij} : \text{role}(i) \neq \text{role}(j)\} \quad (8)$$

- Aggregate:** We report the mean within-role correlation ($\bar{\rho}_{\text{within}} \approx 0.24$) and mean across-role correlation ($\bar{\rho}_{\text{across}} \approx 0.10$). The difference $\Delta\rho = \bar{\rho}_{\text{within}} - \bar{\rho}_{\text{across}}$ measures functional grouping strength.

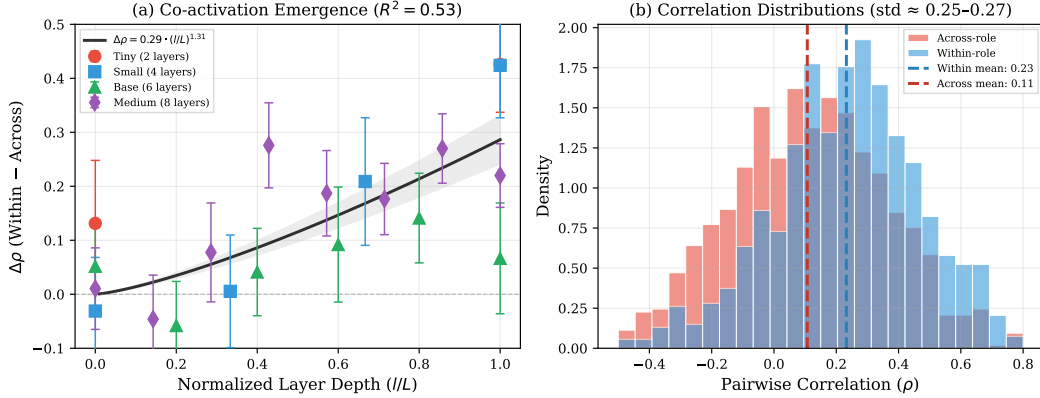


Figure 5: Role-specific neuron separation is weak but increases with depth. *Top*: Each point shows $\Delta\rho = \rho_{\text{within}} - \rho_{\text{across}}$ for one layer, measuring whether same-role neurons co-activate more than different-role neurons. Error bars show approximate standard errors. We fit a power-law $\Delta\rho(l) = \alpha \cdot (l/L)^\beta$, obtaining $\alpha = 0.29 \pm 0.05$, $\beta = 1.31 \pm 0.51$, $R^2 = 0.53$. *Bottom*: The underlying distributions of within-role (blue) and across-role (red) correlations. The distributions heavily overlap ($\text{std} \approx 0.3\text{--}0.4$ vs. mean differences of 0.1–0.2), indicating that role-specific groupings are weak but present.

D Semantic Role Representations Across Scales

We visualize PropBank-style semantic role representations for all model scales using PCA and t-SNE.

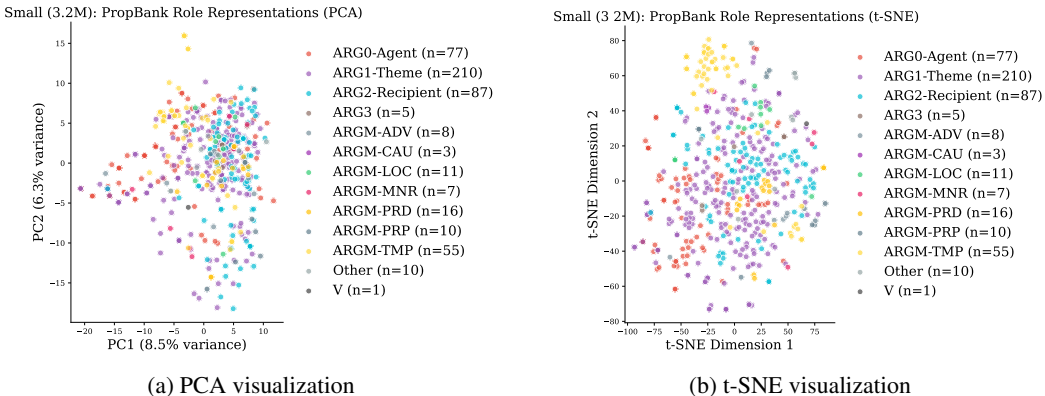


Figure 6: Small model (3.2M transformer parameters): PropBank role representations. Final layer activations colored by PropBank role; ARG0-Agent shows partial clustering, while ARG1 variants and adjuncts are distributed across the space. PCA explains 14.8% of variance in the first two components.

E PropBank Label Assignment

The QA-SRL dataset provides question-answer pairs but not explicit PropBank semantic role labels. To obtain PropBank labels for our analysis, we use AllenNLP’s BERT-based SRL model [Shi and Lin, 2019], specifically the `structured-prediction-srl-bert.2020.12.15` checkpoint trained on OntoNotes 5.0. This model achieves 86.5 F1 on the CoNLL-2012 SRL benchmark.

Labeling Process. For each QA-SRL example (sentence, question, answer), we:

1. Run the AllenNLP SRL predictor on the sentence to obtain PropBank argument structure for each verb.

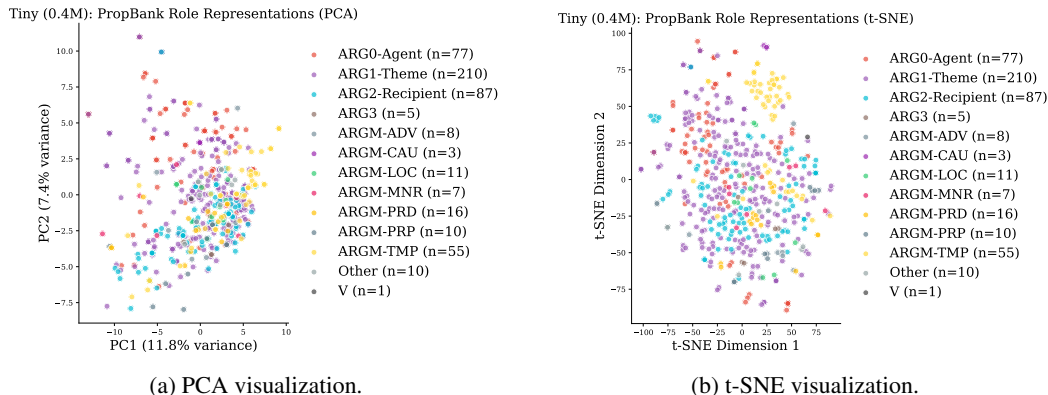


Figure 7: Tiny model (0.4M transformer parameters): PropBank role representations. PCA (left) and t-SNE (right) visualization of final layer activations colored by PropBank role. Even at this minimal scale, ARG0-Agent shows some separation. PCA explains 19.2% of variance in first two components, more than larger models, suggesting simpler/more concentrated representations.

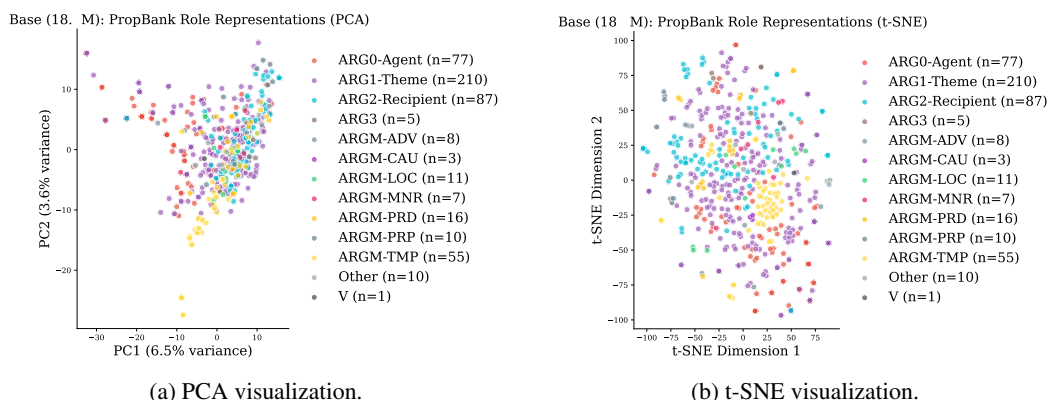


Figure 8: Base model (18.9M transformer parameters): PropBank role representations. PCA (left) and t-SNE (right) visualization of final layer activations colored by PropBank role. Similar to the Small model, ARG0-Agent shows partial clustering, while other roles (ARG1 variants, ARGM adjuncts) overlap substantially. PCA explains 10.1% of variance in first two components.

2. Match the QA-SRL answer span to predicted SRL argument spans using character overlap.
3. Assign the PropBank label if $\geq 50\%$ of the answer overlaps with an SRL argument; otherwise mark as “Unknown.”

Label Categories. For role-conditioned analyses (correlation, neuron-ablation $\Delta F1$) we collapse PropBank labels into the following readable categories:

- **ARG0-Agent:** Proto-agent (doer, causer).
- **ARG1-Theme:** Proto-patient (undergoer, theme).
- **ARG2-Other:** Varies by verb (beneficiary, instrument, attribute, recipient, quantity).
- **ARGM-LOC:** Location.
- **ARGM-TMP:** Temporal/Time.
- **ARGM-MNR:** Manner (how the action was performed).
- **ARGM-CAU:** Cause.
- **ARGM-DIR:** Direction.

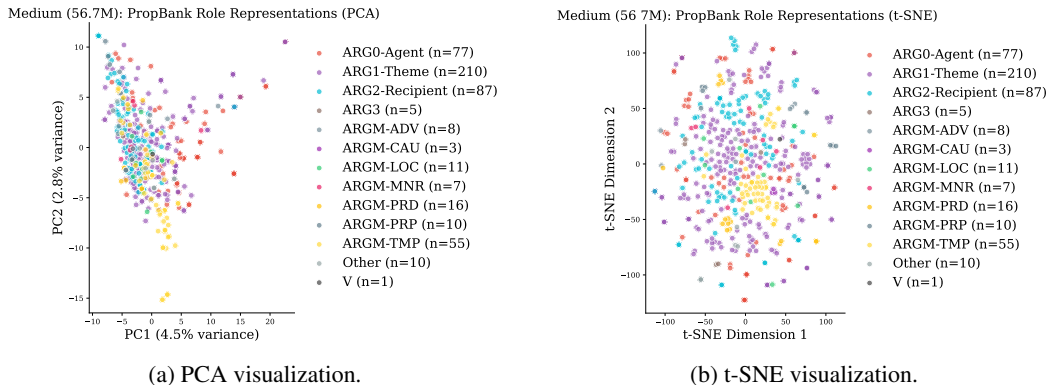


Figure 9: Medium model (56.7M transformer parameters): PropBank role representations. PCA (left) and t-SNE (right) visualization of final layer activations colored by PropBank role. The Medium model shows similar patterns to smaller scales, with ARG0-Agent partially separated but most roles distributed across representation space. PCA explains only 7.3% of variance, suggesting representations become more distributed with scale.

Raw labels in visualizations. The PCA and t-SNE scatter plots in Appendix D (Figures 6–9) and the role-selectivity heatmap in Figure 4 display the full set of raw labels emitted by AllenNLP rather than the collapsed categories above, in order to expose any sub-role structure to the reader. The additional labels visible in those figures (ARG2-Recipient, ARG3, ARGM-ADV, ARGM-PRD, ARGM-PRP, and the Quantity category in Figure 4) are AllenNLP’s verb-specific or adverbial sub-roles. They are subsumed under **ARG2-Other** or treated as out-of-vocabulary noise in the collapsed scheme used for all numerical analyses, so the figures and tables refer to slightly different label inventories by design.

F Replication on GPT-2

To rule out that the Agent-neuron sign reversal is an artifact of our specific training setup, we replicate the causal neuron ablation protocol on OpenAI’s GPT-2 [Radford et al., 2019] at two scales: GPT-2 Small (124M parameters, 12 layers) and GPT-2 Medium (355M parameters, 24 layers). GPT-2 was trained on WebText, providing approximately $80\times$ more tokens per parameter than our custom Medium model and using a different corpus.

Protocol difference: no-retrain ablation. Custom models use *retrain* ablation: weights are zeroed in the pre-trained checkpoint, then the model is fine-tuned on QA-SRL and evaluated. For GPT-2 and Pythia we instead use *no-retrain* ablation: we freeze the pre-trained backbone, train only a QA head (matching the frozen probing protocol), zero the targeted neurons in the resulting probe, and re-evaluate without further training. This is necessary because we do not fine-tune off-the-shelf GPT-2/Pythia in the main protocol (the goal is to probe pre-training, not adapt these large models), and re-running fine-tuning at every ablation site would multiply the compute by orders of magnitude. The two protocols measure related but distinct causal properties: retrain ablation tests whether a neuron is necessary for *learning* the role, while no-retrain ablation tests whether it is necessary for *using* role information already present after probing. We report both signs of the Agent effect across families because the central claim is qualitative (sign attenuation as a function of scale), not a quantitative comparison of $\Delta F1$ magnitudes between families. Random-neuron controls (third column of Tables 10 and 11) show near-zero effects under the no-retrain protocol, ruling out trivial perturbation artifacts.

Layer-wise probing on GPT-2 confirms a depth gradient consistent with Section 4.4: the best probing layer is at 92% depth in GPT-2 Small (layer 11, F1 = 31.2%) and 71% depth in GPT-2 Medium (layer 17, F1 = 35.1%).

Table 10: GPT-2 neuron ablation results (5 seeds each). Agent-neurons are strongly causal in GPT-2 Small (-9.4%) and negligible in GPT-2 Medium (-0.8%), matching the sign-attenuation pattern in our custom models. Random neuron controls show near-zero effects.

Model	Role	No-retrain Δ	Random control Δ
GPT-2 Small (124M)	Agent	$-9.4 \pm 2.1\%$	$+0.1 \pm 0.8\%$
GPT-2 Small (124M)	Time	$-0.5 \pm 0.7\%$	$0.0 \pm 0.5\%$
GPT-2 Medium (355M)	Agent	$-0.8 \pm 0.7\%$	$0.0 \pm 0.5\%$
GPT-2 Medium (355M)	Time	$-3.9 \pm 1.6\%$	$+0.4 \pm 0.6\%$

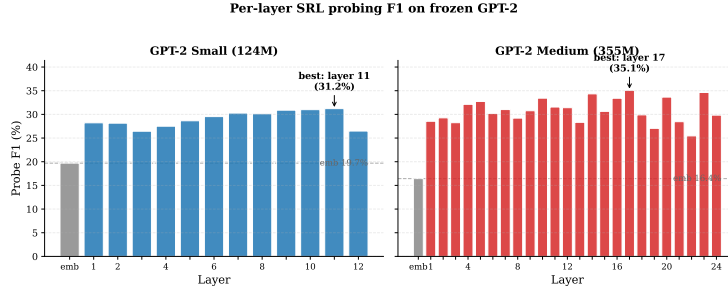


Figure 10: Layer-wise probing F1 on GPT-2 Small and Medium. SRL information peaks in deeper layers, with the best layer at 92% depth (Small) and 71% depth (Medium).

G Replication on Pythia

We further replicate on EleutherAI’s Pythia [Biderman et al., 2023], a third model family trained on The Pile [Gao et al., 2020], a different corpus from both WikiText-103 and WebText. Pythia provides three additional scales (70M, 160M, 410M).

Table 11: Pythia neuron ablation results (5 seeds each). Agent neuron causal effects attenuate from -8.3% at 70M to $+0.5\%$ at 410M, consistent with the sign-attenuation pattern in our custom and GPT-2 results. Random controls confirm role-specificity.

Model	Role	No-retrain Δ	Random control Δ
Pythia-70M	Agent	$-8.3 \pm 1.3\%$	$-0.4 \pm 0.8\%$
Pythia-160M	Agent	$-1.5 \pm 1.1\%$	$+0.2 \pm 0.5\%$
Pythia-410M	Agent	$+0.5 \pm 1.5\%$	$+0.1 \pm 0.6\%$
Pythia-410M	Time	$-1.2 \pm 0.9\%$	$+0.2 \pm 0.3\%$

The depth gradient also holds: the best probing layer is at 17% depth (Pythia-70M), 33% depth (Pythia-160M), and 42% depth (Pythia-410M).

H Component-Level Circuit Analysis

To characterize the transition from concentrated to distributed organization, we zero-ablated each attention layer and MLP layer individually (3 seeds each) across all six models and measured the causal effect on Agent F1.

I Emergence During Pre-training

We probed intermediate pre-training checkpoints (every 5th epoch) across all four custom scales to track when SRL information appears.

Table 12: Component-level circuit analysis. The number of components (attention + MLP layers) needed for 80% of total causal importance increases with scale, while the concentration ratio decreases.

Model	Components for 80%	Total components	Concentration ratio
Custom Tiny (0.4M)	2.3	4	58%
Custom Small (3.2M)	4.7	8	58%
Custom Base (18.9M)	6.3	12	53%
Custom Medium (57M)	7.3	16	46%
GPT-2 Small (124M)	11.3	24	47%
GPT-2 Medium (355M)	21.3	48	44%

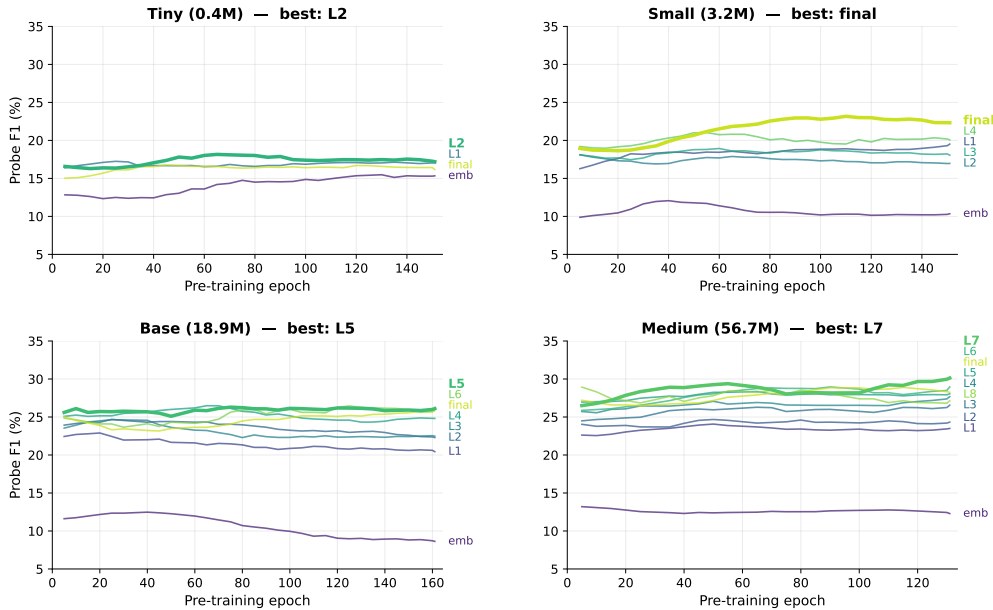


Figure 11: Per-layer probe F1 across pre-training, one panel per scale. Each line is one layer (embeddings, transformer blocks, final norm), labelled at its right endpoint; the best layer per scale is bolded and named in the panel title. F1 stabilises within the first 10–20 epochs and remains roughly flat thereafter, with embeddings persistently ~ 10 F1 below transformer-block layers. Across panels, the best layer deepens with scale (L2 in Tiny, final in Small, L5 in Base, L7 in Medium), and steady-state F1 grows monotonically with scale ($\sim 17\%$ / $\sim 22\%$ / $\sim 26\%$ / $\sim 30\%$).

J Frozen-Embedding (SEP-only) Ablation

To isolate what is encoded in pre-trained transformer weights, we freeze the entire token embedding matrix except [SEP] (kept trainable so the model can disambiguate question from sentence), alongside positional embeddings and transformer blocks; only [SEP] and the QA head update.

The residual 3–4 F1 gap at Base/Medium is smaller than the 12–19 F1 frozen-probe gap, showing the original probe condition combines transformer-encoded emergence with embedding adaptation. Combined with the zero-adaptation per-layer probes (Section 4.4, 10–26% F1), SEP-only establishes that SRL emergence in transformer weights is statistically significant at Base/Medium; at Tiny/Small the single-token bottleneck limits what the SEP-only setup can detect, while the per-layer probes still recover above-chance F1 at those scales.

Table 13: Pre-training convergence status. The Medium model has not converged at its final checkpoint, suggesting our emergence scores are conservative lower bounds.

Model	Final best layer	Probe F1	Status
Tiny (0.4M)	block_1	17.2%	Stable from early training
Small (3.2M)	final_norm	22.5%	Slowly rising
Base (18.9M)	block_5	26.3%	Stable by mid-training
Medium (57M)	block_7	30.8%	Not converged at epoch 131

Table 14: Frozen-embedding (SEP-only) ablation, 5 seeds. With the token embedding matrix held fixed except [SEP], the residual transformer contribution grows monotonically with scale and is significant at Base ($p = 0.004$) and Medium ($p = 0.002$); Tiny/Small are non-significant, reflecting a capacity bottleneck on routing task information through a single trainable token across only 2–4 blocks.

Scale	Pretrained F1	Random F1	Emergence
Tiny	23.9 ± 1.0	24.4 ± 1.3	$-0.5 \pm 1.1\%$ (ns, $p = 0.38$)
Small	27.9 ± 1.1	27.4 ± 0.7	$+0.5 \pm 1.9\%$ (ns, $p = 0.59$)
Base	30.5 ± 0.8	27.8 ± 0.4	$+2.7 \pm 1.0\%$ ($t = 6.2$, $p = 0.004$)
Medium	31.6 ± 0.4	28.0 ± 0.7	$+3.6 \pm 1.1\%$ ($t = 7.5$, $p = 0.002$)